Working Group 2, Deliverable 2.1

PHY design for indoor WA serving multiple users with mobility and for resource-constrained embedded devices within targeted short-range IoT scenarios; Development of high-accuracy OCC/VLC-based indoor localization and sensing techniques in indoor and outdoor smart environments.

Report edited by Giulio Cossu (Scuola Superiore Sant'Anna, Pisa, Italy), Xiaodan Pang (KTH Royal Institute of Technology, Sweden) and Nobby Stevens (KU Leuven, Belgium).

April 2023

Contents

List of Figures

1 Introduction

This document embodies the deliverable 1 of working group 2 of the COST action project no CA19111 with the title NEWFOCUS. It consists of an ordened classification of the research efforts that have been executed by the different action participants during this first part of the project. In accordance to the project proposal, this first working group 2 deliverable is entitled "PHY design for indoor WA serving multiple users with mobility and for resource-constrained embedded devices within targeted short-range IoT scenarios; Development of high-accuracy OCC/VLC-based indoor localization and sensing techniques in indoor and outdoor smart environments." When considering the different domains allocated by this title, we can distinguish three different classes, namely

a) PHY design for indoor WA serving multiple users with mobility and for resource-constrained embedded devices within targeted short-range IoT scenarios

b) Development of high-accuracy OCC/VLC-based indoor localization

c) Sensing techniques in indoor and outdoor smart environments

Along these lines, we have thus created three sections. As one can readily observe, the efforts by the participants have been significant, demonstrating the vivid research domain of short range optical wireless communications.

2 PHY design for indoor WA serving multiple users with mobility and for resource-constrained embedded devices within targeted short-range IoT scenarios

2.1 Detection of Non-Line-of-Sight Contributions for Visible Light Positioning by Polarization

Researchers: *Jorik De Bruycker (KUL, Belgium), Stanislav Zvánovec (CTU, Czech Republic) and Nobby Stevens (KUL, Belgium).*

This contribution investigated the possibility of detecting reflections or non-line-of-sight contributions by means of polarization in the context of Visible Light Positioning. As these may have a detrimental effect on the performance, detecting and/or quantifying these contributions has potential purpose in improving the accuracy of VLP systems. A simple lab setup was constructed as illustrated in Fig. 1 using a modulated LED as a transmitter and a photodiode as a receiver with a linear polarizer mounted in front to measure the received signal strength of the LED transmitter. A reflective surface is added to compare a scenario with non-line-of-sight contributions present to a baseline. The results are shown in Fig. 2 where the measured received signal strength with non-line-of-sight contributions normalized with respect to the line-of-sight only baseline is plotted and a clear dependence on the polarizer angle is visible. These results thus demonstrate the possibility of detecting the non-line-of-sight contributions by employing a polarization diversity receiver.
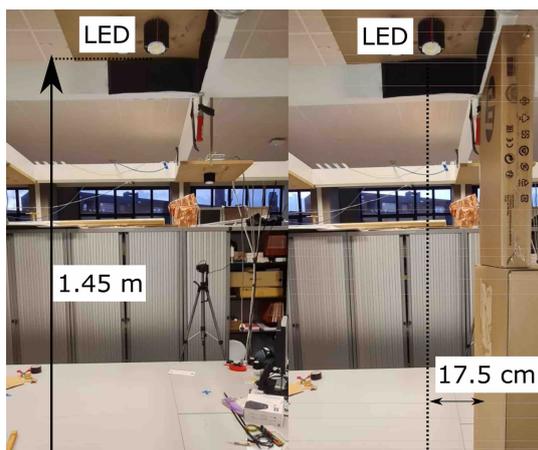
Figure 1: Measurement setup with an LED transmitter and a photodiode receiver.
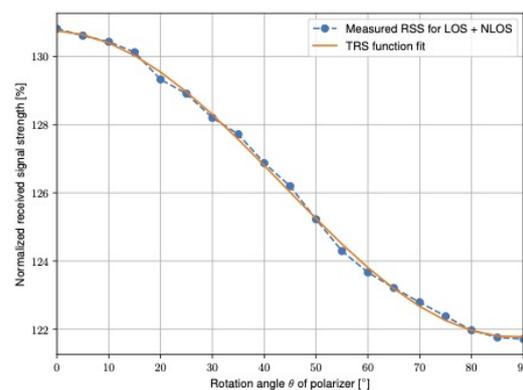
Figure 2: Measured received signal strength for the Non-Line-of-Sight scenario normalized with respect to the baseline measurement.

2.2 Performance Analysis of N-Fisher-Snedecor F Fading and Its Application to N-Hop FSO Communications

Researchers: *Caslav Stefanovic (Universidad Carlos III de Madrid, Spain), Maximo Morales-Céspedes (Universidad Carlos III de Madrid, Spain), Rastislav Róka (Slovak University of Technology in Bratislava, Slovakia), Ana Garcia Armada (Universidad Carlos III de Madrid, Spain)*

The Fisher-Snedecor F distribution has been recently proposed as an experimentally verified and tractable turbulence induced fading model (TIFM) for free space optical (FSO) communications. This paper provides outage probability (OP) and higher-order (HO) performance analysis of the product of N independent but not identically distributed (i.n.i.d) Fisher- Snedecor F random variates (RVs). Accurate and closed-form (C-F) expressions for cumulative distribution function (CDF), level crossing rate (LCR) and average fade duration (AFD) of N-Fisher-Snedecor F distribution are successfully derived. The general property of a Laplace approximation approach for evaluation of N-folded complex integral-form (I-F) LCR expressions has been applied. The obtained statistical results are directly related to the per-

formance evaluation of N-hop FSO communication links. In Fig. 3, the level crossing rate (LCR) for various thresholds is presented. As expected, strong turbulence causes the LCR to take higher values. By shifting from strong-to-moderate or moderate-to-weak turbulence conditions, the LCR decreases. Contrary, the increase in the value of N causes the LCR to increase. In Fig. 4, the average fade duration (AFD) for various thresholds is presented. It can be seen that by increasing the value of N, the AFD increases for lower threshold values, while the AFD decreases for higher threshold values. It can be further observed that by shifting from strong-to-moderate or moderate-to-weak conditions, AFD slightly decreases for lower threshold values.
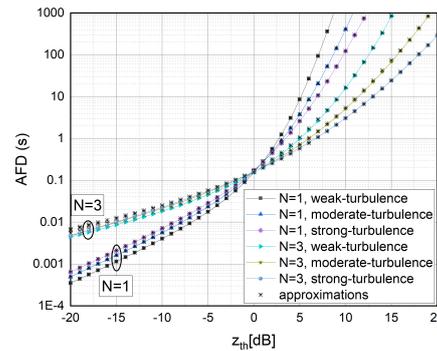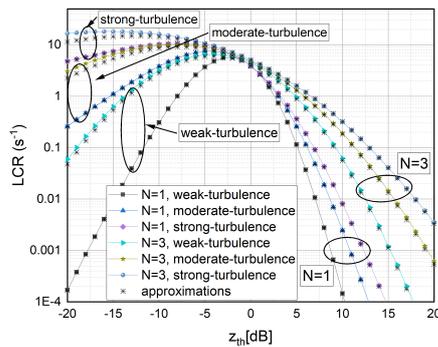
Figure 3: LCR (1/s) of N-Fisher-Snedecor F TIFM observed for weak, moderate and strong turbulence conditions and various N.

Figure 4: AFD (s) of N-Fisher-Snedecor F TIFM observed for weak, moderate and strong turbulence conditions and various N.

2.3 Real-Time MEMS-assisted Beam Steering for Visible Light Communication System.

Researchers: *Juan Apolo (UPV, Spain), Othman Younus (UNN, UK), Beatriz Ortega (UPV, Spain), Vicenç Almenar (UPV, Spain), Zabih Ghassemlooy (UNN, UK).*

In the next generation of mobile communications, 6G, visible light communications (VLC) technology is expected to provide small-to-medium cells with low-to-high data throughputs in densely populated environments in coexistence with traditional RF technology. One of the main challenges addressed by VLC systems is the need for line-of-sight (LoS) between transmitter and receiver, because communications are affected by blockages caused by, for example, human and object movement. Approaches based on the use of beamforming techniques or reconfigurable intelligent surfaces (RIS) can improve the range and reliability of VLC systems [1, 2] by adjusting the intensity and direction of the light to ensure a stronger and more stable connection also when blockages exist. Polymer optical fibers (POF) are designed to operate in the visible spectrum and have several advantages over traditional glass fibers, such as lower costs, mechanical flexibility, and easy installation. Due to these properties, they are well suited to high-speed transmission in indoor communications [3], as well as automotive and industrial applications [4]. As a result, in hybrid wired and wireless networks, the data signal is distributed through the POF and wireless interface using opto-electrical (O/E) and electro-optical (E/O) conversion modules. However, a recent approach based on a passive interface has led to demonstration of free-luminaire VLC point-to-point links [5, 6].

In this contribution, an indoor scenario is considered with a single access point and a mirror-based MEMS technology, acting as a single-element Intelligent Reflecting Surface (IRS). Fig 5 shows the schematic diagram of the MEMS-assisted camera-based tracking VLC system. A single MEMS mirror is employed to redirect a VLC light beam in a luminaire-free system to prevent the loss of LoS in moving users. The optical signal is transmitted and distributed by an in-building POF network where

the wired-wireless optical interface is passive and does not require opto-electrical (O/E) and electro-optical (E/O) (i.e., luminaire-free) since it only uses an optical lenses for beam collimation. Dynamic tracking of the detector by using an optical camera is used to adjust the orientation of the mirror, and therefore, seamless connectivity is guaranteed over an increased coverage area. To implement real-time Rx tracking, algorithms and image processing techniques are used to convert the Rx pixel position in the camera output into room coordinates. Both acquisition and tracking have been implemented using a closed-loop MEMS system.

The performance of the system was evaluated in terms of bit error rate (BER) as a function of the received optical power (RoP) for different data rates and a range of photodetector (PD) gains as shown in Fig. 6. Transmission tests were performed using a random data sequence in the non-return-to-zero on-off keying (NRZ-OOK) scheme. The transmission of a bit rate up to 10 Mbps for an RoP of -31 dBm was demonstrated with an estimated range of 1.67 m wireless link, although smaller bit rates such as 1 Mbps can be used at link distances greater than 2 m.

In this contribution we demonstrated the implementation of a MEMS-assisted camera-based tracking VLC system in a laboratory setup as a proof-of-concept. Real-time Rx tracking was demonstrated by employing a GMM-based background subtraction algorithm, blob analysis, and geometrical transformation to map its position from pixels to the room coordinates. The actual Rx position was sent to the mirror controller to set the corresponding steering angle for detector tracking and therefore, LoS was maintained despite of the user motion. The performance of the system was evaluated in terms of BER as a function of the received optical power. The transmission of a bit rate up to 10 Mbps for a RoP of -31 dBm was demonstrated with an estimated range of 1.67 m wireless link, although smaller bit rates such as 1 Mbps can be used at link distances greater than 2 m using a non-return-to-zero on-off keying (NRZ-OOK) modulation format.
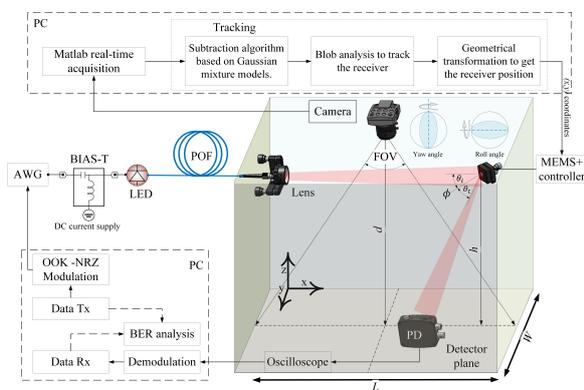
Figure 5: Block diagram of proposed VLC real-time MEMs assisted tracking.
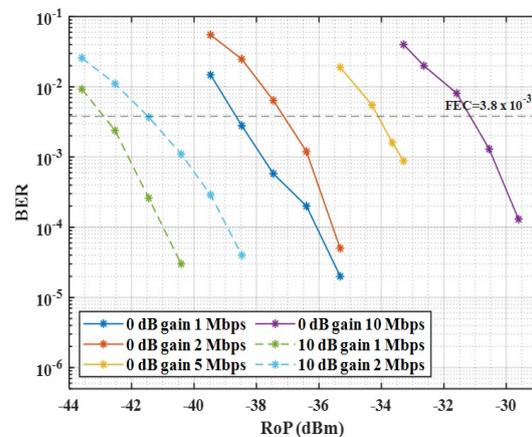
Figure 6: BER performance vs RoP for different gains at the PD.

2.4 Hybrid POF/VLC Links Based on a Single LED for Indoor Communications.

Researchers: *Juan Apolo (UPV, Spain), Beatriz Ortega (UPV, Spain), Vicenç Almenar (UPV, Spain)*

Among different optical wireless communications (OWC) approaches, visible light communication (VLC) is an attractive choice for indoor networks because it offers a huge amount of unregulated bandwidth, high security, low latency, and immunity to electromagnetic interference while using low-cost narrow bandwidth light-emitting diodes (LEDs). Furthermore, recent works demonstrated the interest in heterogeneous networks based on hybrid polymer optical fiber (POF)/VLC links as a converged solution to integrate fiber backbone and in-building networks [7, 8] where large core diameter and small bending

radius of POFs lead to low cost and easy installation.

This contribution proposes a hybrid POF/VLC link based on a single LED for indoor communications. Fig. 7(a) describes the implementation of a POF link as a front-haul downlink solution for feeding the VLC system. The passive optical front-end at the ceiling only includes an optical lens with no optical-to-electric (O/E) and electric-to-optical (E/O) converter. Different signal bandwidths and modulation formats, QPSK, 16-QAM, and 64-QAM, have been transmitted over 1.5 m polymer optical fiber (POF) and 1.5 m free-space optics (FSO).

The transmitter consists of a red commercial LED emitting an optical carrier centered at λ of 650 nm, which is coupled into a 1 mm diameter step-index POF (SI-POF) section employing a micro-lens included in the LED package. The scope is to reduce the beam divergence by optimizing the beam collimation stage of the system. Hence different configurations of lenses in both the transmitter and receiver are being studied. The analysis is limited to low-cost commercial lenses, in order to maximize optical power in the detector.

Fig. 8 compares maximum achievable throughputs in terms of distance for different lens configurations. A maximum throughput of 294 Mb/s can be achieved at 1.5 m, but as distance is increased, the received optical power (RoP) worsens and, since the noise level is fixed, the modulation bandwidth must be reduced, accordingly, giving a reduced bit rate. It can be seen that up to 2 m distance, 64-QAM is the best option giving throughputs higher than 200 Mb/s. For longer distances, the signal-to-noise ratio (SNR) reduction requires the use of QPSK with lower bandwidths as the distance increases, giving at 2.8 m a bit rate of 80 Mb/s, which is also suitable for industrial connectivity. At lower distances the QPSK throughput is limited by the 110 MHz maximum bandwidth of the employed components.

This contribution has proposed the use of a centralized LED for indoor communications. Demonstrating a fiber/wireless link without intermediate O/E or E/O conversion stages. The experimental demonstration has validated the design results with excellent agreement between geometrical optics simulation and experimental measurements. As a result, a 294 Mb/s VLC system at 1.5 m wireless link using a 64-QAM modulation scheme has been experimentally demonstrated.
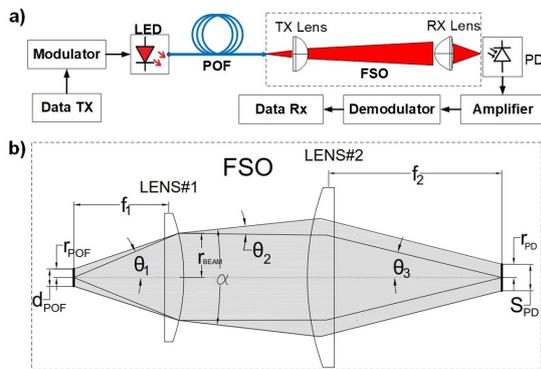
Figure 7: General scheme of the hybrid link: (a) block diagram of the experimental setup for the POF-VLC system, and (b) detail of FSO block: ray tracing diagram.
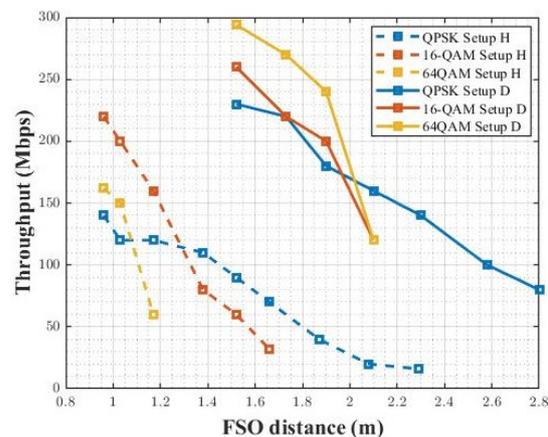
Figure 8: Throughput vs. FSO distance for different modulation formats.

2.5 Performance Analysis of the FBMC Modulation Format in Optical Fiber and Wireless Communications

Researchers: *Rastislav Róka (Slovak University of Technology in Bratislava, Slovakia), Caslav Stefanovic (Universidad Carlos III de Madrid, Spain), Maximo Morales-Céspedes (Universidad Carlos III de Madrid, Spain), Ana Garcia Armada (Universidad Carlos III de Madrid, Spain)*

The FBMC is among the currently most researched techniques for signal processing and is explored

here for passive optical access networks. This paper presents a performance analysis of the FBMC modulation format for applying in optical fiber and wireless communications. For analyzing, we realized simulation models that are based on well-known characteristics of the optical transmission medium and the free space environment that can describe mutual relations between optical signals and environmental influences. In Fig. 9, it is presented a complete block scheme for the optical wireless transmission path including main optical components. The FBMC model can be consequently applied for a purpose of advanced simulations performed in the complete optical transmission path. In Fig. 10, a concrete example of the eye diagram related to transmitted QPSK optical signals using the FSO system for the 1 km path length and the 500 m visibility is introduced. The results suggest that the FBMC format can be utilized for reliable optical fiber and wireless communication systems. The FBMC modulation format utilizing internal multi-level and multi-state modulations can be effectively incorporated into the optical transmission path with both transmission media, thereby more effective utilization of the bandwidth can be achieved, resulting in higher transmission rates of optical signals.
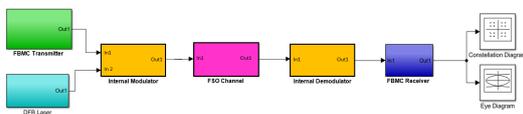
Figure 9: The FBMC model in the OWC.
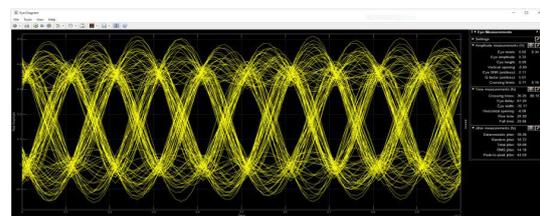
Figure 10: The eye diagram for transmitted QPSK optical signal using the FSO system.

2.6 Analog Multi-Band Carrierless Amplitude and Phase Modulation for Visible Light Communication-Based Internet of Things Systems

Researchers: *Luís Rodrigues (Instituto de Telecomunicações - Aveiro, Portugal), Mónica Figueiredo (Instituto de Telecomunicações - Aveiro, Portugal), Luís Nero Alves (Instituto de Telecomunicações - Aveiro, Portugal), Zabih Ghassemlooy (Northumbria University, United Kingdom)*

In the paper, a multi-user Internet of Things (IoT) system based on carrierless amplitude and phase (m-CAP) modulation, and several bands of visible light communication (VLC) is presented. Aiming at low-cost, low-power, and compact IoT devices, the proposed architecture makes use of analogue receivers and a digital m-CAP modulator fitted in a ceiling LED light fixture. The architecture performance was assessed with respect to the filtering stage design and the existence of guard bands. We explored multiple combinations of emitter and receiver filters – the digital m-CAP modulator pulse shaping filter $p(t)$ considered raised cosine filters as well as digital matched filters for the analogue Bessel and Butterworth filters, both tested in the analogue receiver. Two strategies were taken into consideration in relation to the guard bands: either employing the higher cosine roll-off factor (bandwidth compression) or suppressing the even bands. The Bit Error Rate (BER) performance was obtained by simulation. The system performance was enhanced by using a matched filter in the digital emitter, particularly for Bessel filters, and a remarkable BER performance was attained with a 0.5 dB Eb/No gain loss when compared to the theoretical QAM modulation BER curve in the presence of AWGN. The best results with contiguous modulated bands was obtained when using a raised cosine filter with $\beta = 1$ as $p(t)$ and an analogue Bessel filter, see Fig.11. As an alternative to use the raised cosine filter, guard bands need to be employed to reduce inter-band interference. As can be seen in Fig.12, the results showed that by suppressing the even bands, the BER performance was equal to that of scenarios in which only one band was modulated. As a result, comparable to in the case of a single modulated band, the best performance was obtained when an analogue Bessel filter was used as $p(t)$ together with a digital matched Bessel filter. The results of the study demonstrated the viability of a VLC-based IoT system, achieving a BER similar to the completely digital version employing a digital m-CAP modulator and analogue receivers. Guard bands, a synchronism loop in the analogue receivers, and improved inter-band interference rejection were needed

to increase the system BER. In particular, the proposed architecture could achieve a BER lower than 10^{-3} for an Eb/No of 6dB employing a third-order analogue Bessel filter and a properly synchronised quadrature mixer.

To evaluate system performance, eye patterns, Rx constellations, EVM, and BER were obtained with an experimental setup. The BER vs. distance and the BER vs. Tx/Rx angle LOS scenarios were considered. The BER performance is resilient in the presence of Tx/Rx misalignment, particularly for shorter distances where the device tilt can go as high as 45°and still achieve a BER within the FEC limit. The result is particularly significant given that typical LED lighting fixtures often have a larger radiation pattern, which minimises the impact of Tx/Rx misalignment in real-world scenarios. An improved SNR is expected in testbeds based on commercial lighting fixtures since the LED utilised in the experimental validation is rated at 1 W, which has a lower power when compared to the power ratings of the current lighting systems.
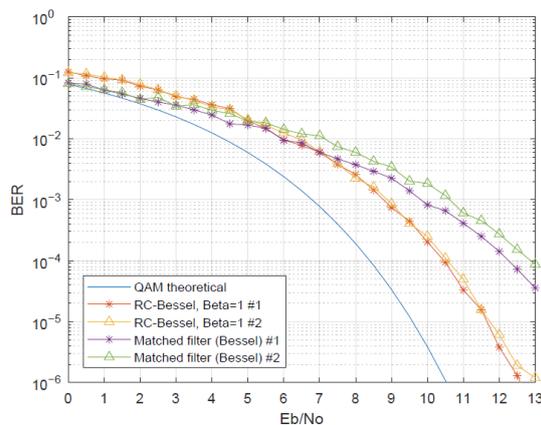
Figure 11: BER comparison with inter-band interference – Rx filter is a third-order Bessel; $p(t)$ was tested with both the raised cosine filter and the matched Bessel filter.
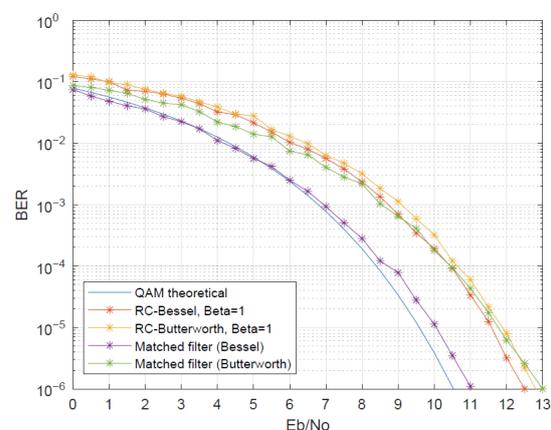
Figure 12: BER using guard bands, by suppressing the even bands.

2.7 Carrierless Amplitude-Phase Modulation for VLC

Researchers: *Mike Wolf, Martin Haardt (Ilmenau University of Technology, Germany)*

If the LEDs used for VLC also serve as lamps for lighting purposes, then the modulation of the LEDs must not cause any perceptible flickering. Below about 200 Hz, the optical power is hardly allowed to vary, although the modulation takes place precisely by varying the optical instantaneous power.

Serial pulse-amplitude modulation (PAM) with a unipolar signal constellation and a rectangular baseband waveform is a popular solution for intensity modulation, but it has to be combined with some kind of line coding to ensure DC-balance. Ternary PAM could be combined, for example, with a 8B6T code [9]. Here, 8 message bits are mapped to 6 ternary symbols, which means that out of $3^6 = 729$ possible code words only a subset is used, namely those that are (almost) DC-balanced. The price, however, is not only additional redundancy, but also that the FEC scheme must be combined with hard-decision.

Another possible solution is to first generate modulated passband signals. These inherently have no spectral components at $f = 0$ (or near $f = 0$), but can only be used to modulate the LED current after adding a DC offset. For serial passband transmission, *Carrierless amplitude-phase (CAP)* modulation and quadrature amplitude modulation are the most prominent approaches. However, since the center frequency of the bandpass waveform only needs to be large enough to avoid frequency components below ≈ 200 Hz, it is obvious not to upconvert a baseband signal by quadrature-modulation. Instead, a

root-raised cosine *passband* pulse (rolloff factor $r_{\cos}$)

$$\psi_{\mathrm{c}}(t) = \psi_{\mathrm{b}}(t)\exp(j2\pi f_{\mathrm{c}}t), \text{ where } \int \psi_{\mathrm{c}}^2(t)\mathrm{d}t = 1 \text{ and } f_{\mathrm{c}} = \frac{1}{2T}(1 + r_{\cos}),$$

is generated with every modulation step $T = \log_2(M)/R_{\mathrm{b}}$ according to

$$p_{\mathrm{tx}}(t) = P + \hat{p}_{\sim}(t) \text{ with } p_{\sim}(t) = \sqrt{2}\cdot\mathrm{Re}\left\{\sum_k x_k \psi_{\mathrm{c}}(t - kT)\right\},$$

where $p_{\sim}(t)$ is the passband component of the ideal CAP signal. The signal $\hat{p}_{\sim}(t)$ is obtained from $p_{\sim}(t)$ by symmetrically cutting all amplitudes of $|p_{\sim}(t)|$ that exceed the mean optical transmit power P. Fig. 13 shows the required optical power P for different modulation orders M of the complex symbols x_k, a target BER of 10^{-3}, optimal clipping and a noise power spectral density N_0. The additive noise is a signal-independent current generated at the photodiode output, where the diode has a responsivity R (in A/W), see Fig. 14. As the electrical energy per bit (in A^{2}s) at the photodiode output depends on $(PR)^2/R_{\mathrm{b}}$, where R_{b} is the bit rate, the BER-performance is a function of $(PR)^2/(R_{\mathrm{b}}N_0)$.

The required $(PR)^2/(R_{\mathrm{b}}N_0)$-ratio is shown as a function of the normalized bit rate $R_{\mathrm{b}}/f_{3,\mathrm{Gauss}}$. The term $f_{3,\mathrm{Gauss}}$ is the 3 dB cutoff frequency of a Gaussian lowpass filter, measured in the optical domain. The lowpass has been introduced in the transmission chain in order to take into account bandwidth limitations, primarily due to the LED(s). The curves would be much flatter if a first-order lowpass had been inserted instead of a Gaussian low pass as suggested in [10]. It should be noted that zero-forcing equalization, realized in the frequency domain, has been assumed. Otherwise, data rates beyond $f_{3,\mathrm{Gauss}}$ would be practically impossible.

The results show that CAP modulation is a very good alternative to PAM, if PAM needs to be combined with line coding. For $R_{\mathrm{b}}/f_{3,\mathrm{Gauss}} > 2$, CAP generally requires a little less power. However, the good performance can only be achieved, if clipping is used. For $M = 16$, for example, all signal amplitudes of $p_{\sim}(t)$ exceeding $2\sqrt{\overline{p_{\sim}^2(t)}}$ need to be clipped. Finally, it should be noted that zero-forcing equalization has been used here only for a first comparison. If the postcursor ISI is removed with a decision-feedback equalizer instead, the results for $R_{\mathrm{b}}/f_{3,\mathrm{Gauss}} > 2$ are significantly better.
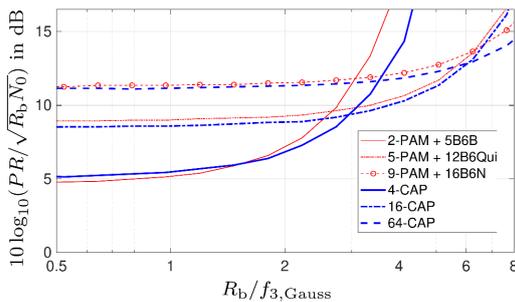
Figure 13: Performance of NRZ-PAM vs. CAP
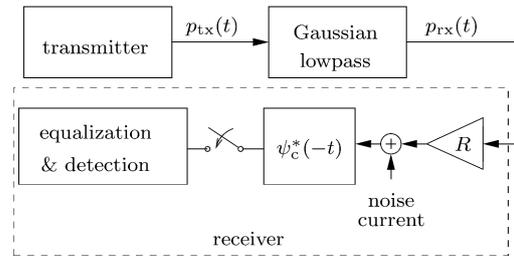
Figure 14: System modeling for CAP transmission. The results are based on $r_{\cos} = 0.2$.

2.8 Optical wireless audio headset for communication in an aircraft cockpit

Researchers: *P. Combeau (XLIM laboratory, University of Poitiers, France), A. Julien-Vergonjanne (XLIM laboratory, University of Limoges, France), S. Sahuguède (XLIM laboratory, University of Limoges, France), L. Aveneau (XLIM laboratory, University of Poitiers, France), H. Boeglen (XLIM laboratory, University of Poitiers, France)*
This contribution investigates the development of an electronic tablet and an audio and connected wireless headset dedicated to pilots for a use inside the aircraft cockpit (cf. Fig. 15), to provide them more comfort during long-haul flight and critical operations as take-offs and landing.

We address these challenges by a simulation approach, based on an advanced modeling of the optical channel. It is characterized by Monte-Carlo Ray-Tracing simulation realized in a realistic 3D model of the cockpit and the crew members. The specific impacts of materials reflectivity, as well as the bodies mobility and the level of geometrical details of the cockpit model are investigated. We show that these key parameters have no impact on the optimal half power semi-angle of the Leds. At the contrary, they are of high importance to realistically evaluate communication performance, in term of needed emitted optical power for instance, as shown on Fig. 16. Then, communication performance are evaluated based on an efficient modulation scheme. The link between needed emitted power and targeted level of communication performance is highlighted, and the contribution of spatial diversity at the headset side is investigated. Finally, the latency is evaluated based on the 802.11 medium access control protocol using distributed coordination function mechanism. In this context, we propose an approach to discuss the trade-offs for different modulation orders, targeted packet error rate, maximal admissible delay or emitted power.
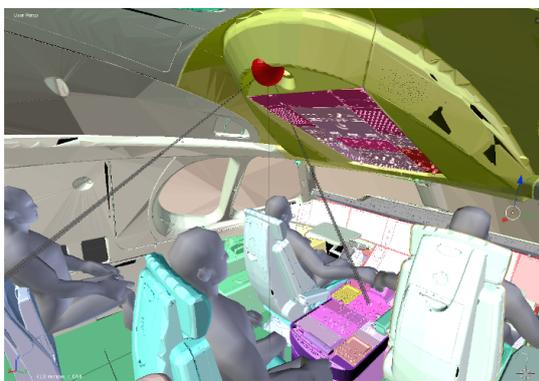
Figure 15: 3D model of an Airbus 350 aircraft cockpit.
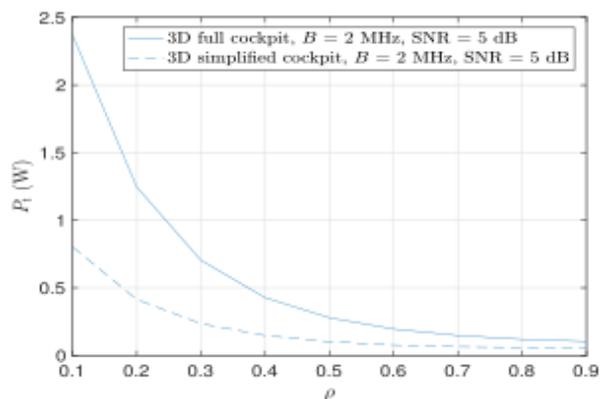
Figure 16: Impacts of material reflectivity and geometry on the needed emitted power.

2.9 Optical characterization of materials

Researchers: *P. Combeau (XLIM laboratory, University of Poitiers, France), L. Aveneau (XLIM laboratory, University of Poitiers, France), P. Thuillier Le Gac (XLIM laboratory, University of Poitiers, France), and R. Xiao (XLIM laboratory, University of Poitiers, France)*

This contribution presents recent researches which address the optical characterization of materials making up an indoor propagation environment. Although being a very impacting parameter for light wave simulation algorithms based on Monte-Carlo Ray-Tracing, as it is shown in Fig. 17, the materials albedos are usually poorly known. To estimate them, conventional approaches use complex and costly measurement frameworks, and it is consequently difficult to envisage exhaustive characterization of materials, especially in situ. This contribution aims to propose a new and more generic approach, usable in situ and based on simple and low-cost framework. This approach uses both numerical simulations and simple and low cost measurements, feeding a genetic algorithm in order that simulated data fit measured ones. A theoretical validation of the concept is realized considering simulated data as virtual measurement, which shows a very good agreement between estimated and true parameters of the materials composing the propagation environment, as illustrated in Fig. 18.

2.10 Two-Tier Multi-Rate Slotted ALOHA for OWC/RF-Based IoT Networks

Researchers: *Milica Petkovic (UNS, FTN, Serbia), Dejan Vukobratovic (UNS, FTN, Serbia), Andrea Munari (DLR, Germany), Federico Clazzer (DLR, Germany)*

In this contribution, we considered a massive IoT scenario where indoor IoT devices access the network via OWC IoT systems that relay data via a backhaul LP WAN. Novel two-tier multi-rate Slotted ALOHA
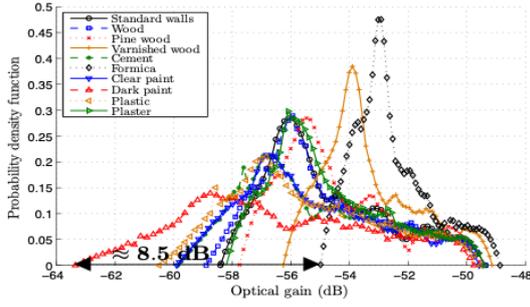
Figure 17: PDF of the received optical gains inside a room according to different materials composing it.
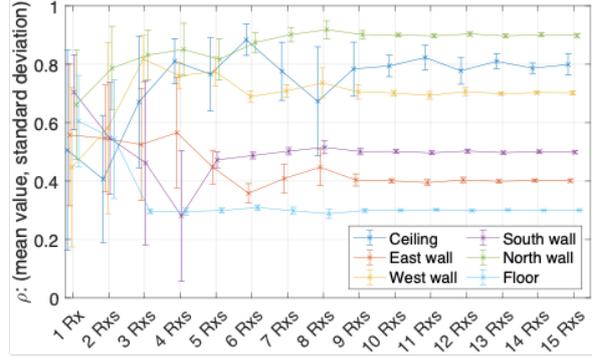
Figure 18: Estimated ρ values according to the number of considered receivers.

system model was proposed in order to design and analyse such hybrid OWC/RF networks, while introducing different slot rates at the OWC and RF tiers. For a particular setup shown in Fig. 19, an overall throughput was investigated to provide insights into the proposed multi-rate OWC/RF SA system design while focusing on the indoor OWC system parameters. The throughput analysis indicates a trade-off between the OWC system parameters, activation probability of IoT devices and slot rate factor M, for the system performance optimization. For example, from Fig. 20 it can be concluded how the semi-angle $\Phi_{1/2}$ affects the overall throughput for different parameter M. Given that most of the parameters may be beyond control of the system designer, we note that controlling M is an elegant way for the proposed two-tier system to operate at favourable throughput.
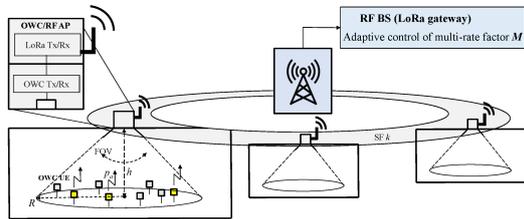
Figure 19: Two-Tier OWC/RF-Based IoT Network.
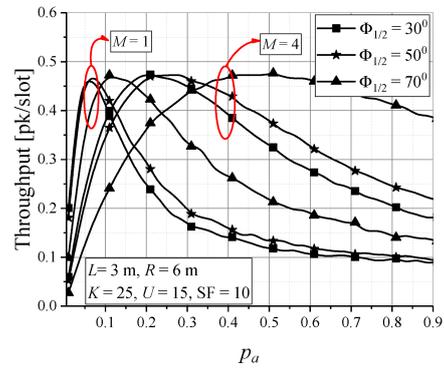
Figure 20: Throughput vs. p_a for different values of semi-angle $\Phi_{1/2}$.

2.11 Slotted Aloha with Capture for OWC-based IoT: Design and Analysis in Finite Block-Length Regime

Researchers: *Tijana Devaja (UNS, FTN, Serbia), Milica Petkovic (UNS, FTN, Serbia), Dejan Vukobratovic (UNS, FTN, Serbia), Francisco J. Escribano (Alcalá de Henares, Spain), Cedomir Stefanovic (AAU, Denmark)*

This contribution proposed a Slotted ALOHA inspired solution for an indoor OWC-based IoT system. This work comprised a communication scenario in which a total U IoT devices equipped with OWC transmitters contend to access a common OWC access point (AP). The transmitting IoT devices are uniformly placed on a horizontal plane, while the OWC AP is located at the ceiling, at a fixed location. With assumption that the OWC receiver exploits the capture effect, the error probability of decoding a short-length data packet originating from a randomly selected OWC IoT transmitter was derived. The

presented analysis includes the derivation of the signal-to-noise-and-interference-ratio (SINR) statistics and usage of finite block-length (FBL) information theory, from which relevant error probability and throughput are derived. Derived expressions were used to obtain numerical results which are further utilized to characterize the trade-offs between the system performance and the OWC system setup parameters. As presented in Figs. 21 and 22, the indoor OWC-based system geometry has an significant impact on the system performance. Also, from Fig. 21 can be concluded that maximal throughput (different for various OWC system setups) exists for optimal value of devices' activation probability, which can be important for the system design to optimize the performance of the SA-based random access protocol.
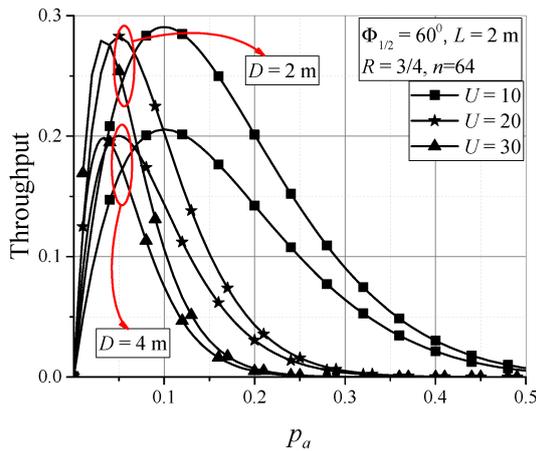
Figure 21: Throughput vs. p_a for different number of IoT devices and radius D.
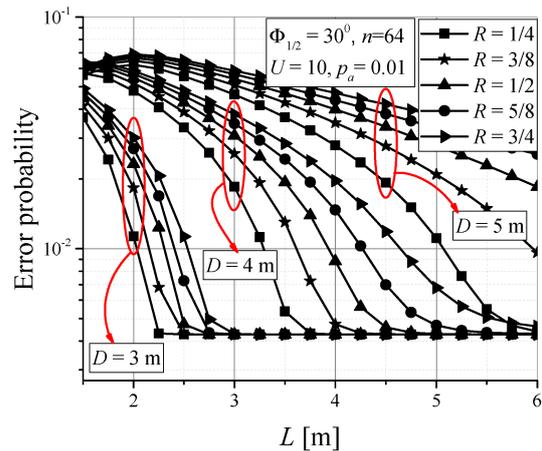
Figure 22: Error probability vs. L for different values of rate R and radius D.

2.12 Slotted Aloha with Capture for an Optical Wireless Communication in Internet of Underwater Things Scenario

Researchers: *Milica Petkovic (UNS, FTN, Serbia), Dejan Vukobratovic (UNS, FTN, Serbia), Sotiris A. Tegos (AUTh, Greece), Panagiotis D. Diamantoulakis (AUTh, Greece), George K. Karagiannidis (AUTh, Greece), Cedomir Stefanovic (AAU, Denmark)*

This contribution proposed a Slotted ALOHA solution for OWC-based Internet of Underwater Things (IoUT) system, where user devices exchange data with an AP which exploits the capture effect. As it is presented in Fig. 23, this work considered scenario where the space spanned by the IoUT nodes is three dimensional, i.e., users are located in half-sphere centred at the AP, which is placed at the bottom of some object on the water surface. The analytical expressions for the system throughput and reliability expressed in terms of the outage probability are derived. Based on the simulated SINR statistics and derived analytical expressions, numerical results are presented and used to investigate the trade-offs between the performance and the IoUT system parameters (number of users, activation probability and type of water medium). For example, Fig. 23 shows throughput dependence on users' activation probability p_a for different values of the total number of IoUT devices U in different water media. Higher p_a and/or higher U imply more active users in a slot, which determines the overall SINR and has a direct effect on the potential of the capture. It can be observed that maximal value of throughput exists for an optimal value of p_a, which depends on the water media. Presented conclusions can provide valuable insights into the design of an SA-based solution for IoUT communications.

2.13 Characterization and Modeling of Lighting White LEDs for VLC Data Link Evaluation

Researchers: *P. Salvador (UPV, Spain), V. Almenar (UPV, Spain), J. Valls (UPV, Spain), J.L. Corral (UPV, Spain), MJ. Canet (UPV, Spain), B. Ortega (UPV, Spain)*
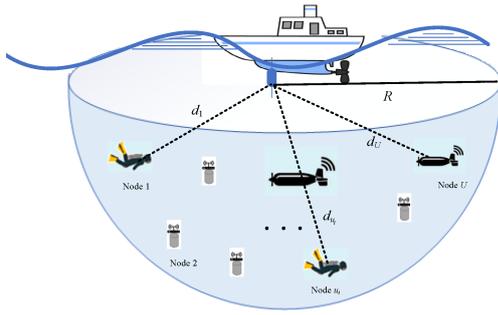
Figure 23: OWC-based IoUT system model.
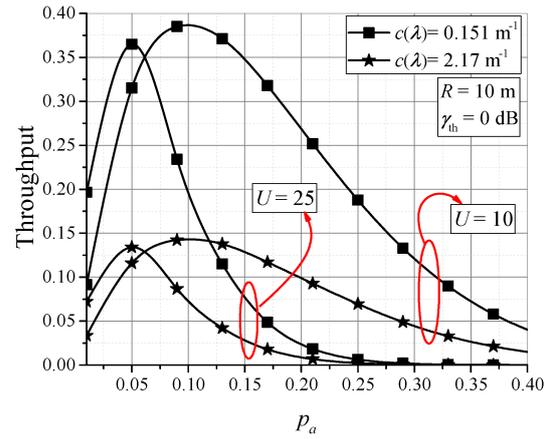
Figure 24: Throughput vs. p_a for different values of underwater coefficient $c(\lambda)$.

In this work, we analyze and model the behavior of high luminous phosphor-coated white LEDs; the main contributions are: i) A model for white LEDs that separates blue diode and phosphor coating effects. A 2nd-order transfer function is considered to characterize the blue diode, which is required to represent the behavior of the LED in a realistic lighting environment. ii) A compact expression for the linear model of the white LED, which includes three poles and one zero. The poles are directly obtained from the frequency response of the blue and the yellow light components. The frequency of the zero is shown to depend on the power ratio of the detected blue and yellow lights and its influence in the white LED frequency response partially counterbalances the effect of the blue LED higher pole. iii) A systematic method to extract the parameters of the model, which requires only three frequency response measurements. This method was validated using three high luminous flux white LEDs with different features.

The proposed linear model for the white LED shown in Fig. 25 is based on a linear combination of the detected blue and yellow light components, modeled as $H_b(s)$ and $H_y(s)$. It is formulated as: $H_w(s) = \gamma_b \cdot H_b(s) + \gamma_y \cdot H_y(s)$, where γ_b and γ_y are the weights with which the blue and yellow components are added at the receiver, respectively. These weights take into account not only the relative proportion of both blue and yellow components in the white light, but also the different responsivities of the photodetector at each wavelength.

After measuring the model parameters of an LED from Cree (CXB1830-0000-000N0BV265E) the frequency response of the system is derived and compared with the measured one. As can be observed in Fig. 26, there is a very good match between the proposed model and the measurements. The slight disagreement at high frequencies is due to the high attenuation (above 40 dB) suffered by the detected signal at those frequencies, which rendered noisier measured values.

2.14 Coverage Optimization With Beamsteering-Based Indoor Optical Wireless Communications

Researchers: *Haitham AL Satai (LISV-UVSQ, France), Bastien Béchadergue (LISV-UVSQ, France), Luc Chassagne (LISV-UVSQ, France) and Wafaa Mohammed Ridha Shakir (ATU, Irak)*

Optical wireless communication (OWC) systems for indoor networking usually rely on cells generated by fixed access points, so that they often experience a strong quality of service degradation because of frequent handover and inter-cell interference. To overcome these problems, steerable optical antennas may be used at both the infrastructure and user levels. Although such beamsteering solutions have already been explored experimentally, there seems to be no thorough comparison of the performance
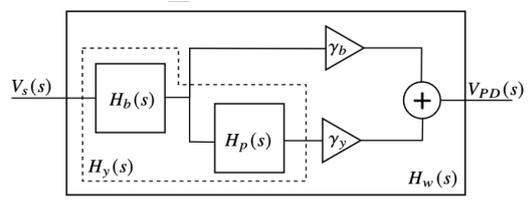
Figure 25: Block diagram of the complete model.
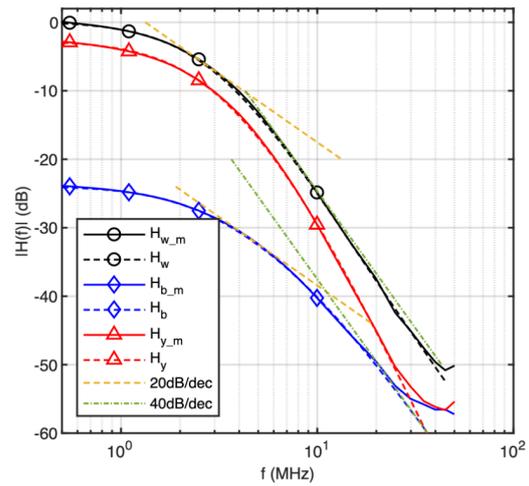
Figure 26: Measured (solid line) and estimated (dashed line) frequency response of LED.

of such a system, especially in terms of coverage, compared to conventional solutions based on fixed antennas.

This work thus aims to provide such a comparison by simulating the three scenarios ('with beamsteering', 'without beamsteering', and with 'manual orientation') represented on Fig. 27, for each of which the bit error rate of a multiband carrierless amplitude phase (m-CAP) modulation signal received by a user moving across a 20×20 m receiving plane at 0.85 m from the floor is estimated. The parameters of this source, its directivity and emission optical power, in particular, are carefully chosen to meet photobiological regulations.

Figure 28 shows in the three scenarios the evolution of the coverage area, defined as the zone where the bit error rate (BER) remains below a threshold of 3.8×10^{-3}, as a function of the semi-angle at half power $\Phi_{1/2}$ of a 1 W optical source. It appears clearly that 'with beamsteering', a large increase in coverage is obtained compared to the cases where it is not or partially used. However, the interest of beamsteering gets lower as the directivity of the source gets larger, even though in the worst case, a threefold increase in coverage is still obtained.

2.15 Joint Visible Light Sensing and Communication Using m-CAP Modulation

Researchers: *Lina Shi (LISV-UVSQ, France), Bastien Béchadergue (LISV-UVSQ, France), Luc Chassagne (LISV-UVSQ, France) and Hongyu Guan (LISV-UVSQ, France)*
As 5G devices and networks continue to roll out, new broadcasting services and capabilities have been introduced to the entire ecosystem, opening up additional new applications and granular business opportunities, where indoor joint communication and sensing are critical. Under this trend, in this work, we propose a new system using multi-band carrierless amplitude and phase (m-CAP) modulation associated with received signal strength (RSS)-based trilateration to achieve visible light sensing and communication from the same signal. The light source limitations in terms of dynamic range and modulation bandwidth are especially taken into account using data from actual components.

The proposed system is eventually composed of 9 access points distributed across the ceiling of a 4×4×2.5 m room, which provide according to MATLAB simulations an illuminance between 300 and 500 lux over a receiver plane 85 cm above the floor. At the same time, positioning is possible with an error lower than 7.17 cm in 90 % of the cases, and a continuous data connectivity at 32 Mbps is ensured over the whole room, as represented respectively on Fig. 29 and Fig. 30.

The influence of several parameters, including that of the main m-CAP settings, on this performance

(a) Scenario 'with beamsteering' ($\phi = \psi = 0$).

(b) Scenario 'without beamsteering' ($\phi = \psi$).

(c) Scenario with 'manual orientation' ($\phi \neq \psi$).
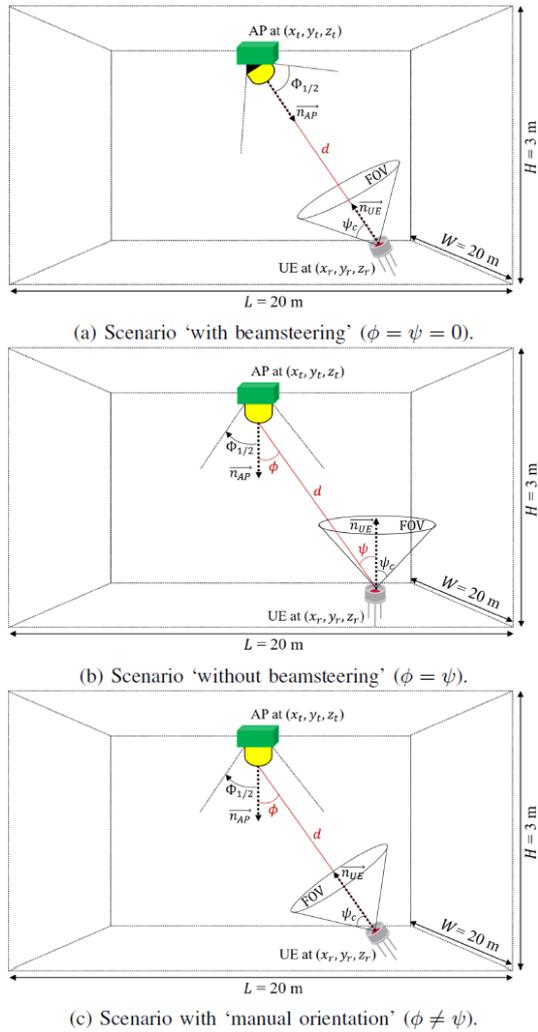
Figure 27: Indoor OWC scenarios considered.

(a) All scenarios.
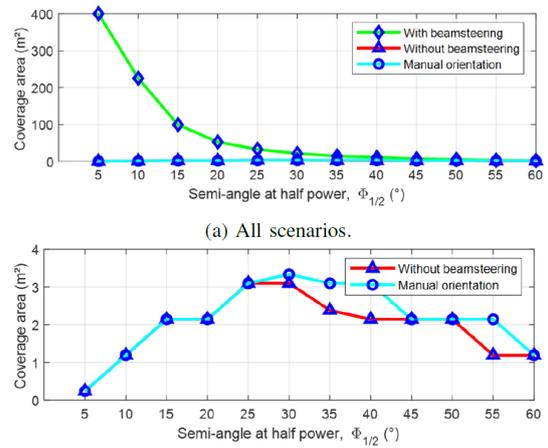
Figure 28: Coverage area versus semi-angle at half power $\Phi_{1/2}$ when the source optical power is 1 W.

is also studied in order to define some general rules for the design of such a system. Results show that the positioning error depends strongly on the bias current of the access points but marginally on the number of m-CAP sub-bands m, the m-CAP filters span L_{SPAN} and roll-off factor α, whereas the communication performance increase with m, α and L_{SPAN}, however at the cost of complexity.
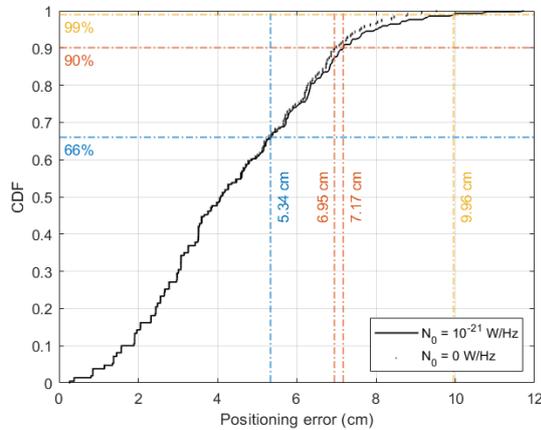
Figure 29: Cumulative distribution function of the positioning error.
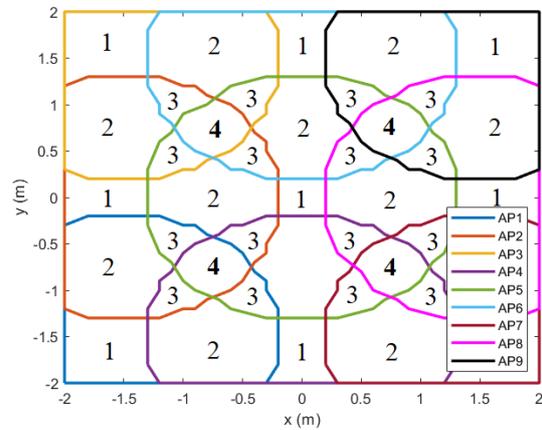
Figure 30: Coverage area of each access point when used successively and not together to transmit a data signal. The numbers indicate the number of overlapping coverage areas.

2.16 Closed form approximation of the actual spectral emission of commercial color LEDs for VLC

Researchers: *Alexis Dowhuszko (Aalto University, Finland), Borja Genovés Guzmán (IMDEA Networks Institute, Spain).*

The approximations reported so far in the literature to model the spectral power emission of color LEDs are not good enough to estimate Key Performance Indictators (KPIs) of Visible Light Communications (VLC) systems. Most of these spectral emission models were studied from a purely empirical perspective, without paying much attention to the tails of the spectrum, which is critical to assess correctly the impact of the (inter-color) cross-talk interference, or estimate the Correlated Color Temperature (CCT) and/or Color Rendering Index (CRI). Starting from the theoretical spectral emission of a color LED, a closed form expression was derived based on an asymmetric Pearson type-VII function, which is shown to approximate accurately the measured spectra of the color LEDs at different working regimes. Moreover, the parameters that defined the shape of the approximation were obtained from three representative values, namely the peak wavelength and the lower (and upper) half-maximum wavelengths. The effect of the DC-bias current on the these three parameters were also studied, and low-order polynomial approximations were derived to estimate these parameters at different working regimes. Finally, the accuracy of the asymmetric Pearson-VII model was validated using the step-size of the MacAdam ellipses.

Figures 31 and 32 show the goodness of the proposed asymmetric Pearson-VII approximation for the six color LEDs under study at DC-bias points (i.e., $I_{dc} = 60$ mA, 100 mA, and 200 mA). As expected, there are no major differences between the closed form approximations and the measured spectral power emissions in the whole range of wavelengths that correspond to the visible light band. In addition, it is shown that the parameters of these distributions (i.e., peak wavelength, left-and half-side half-maximum wavelengths, and peak spectral emission) can be accurately estimated using low-order polynomial approximations, whose coefficients can be computed using MMSE interpolation.
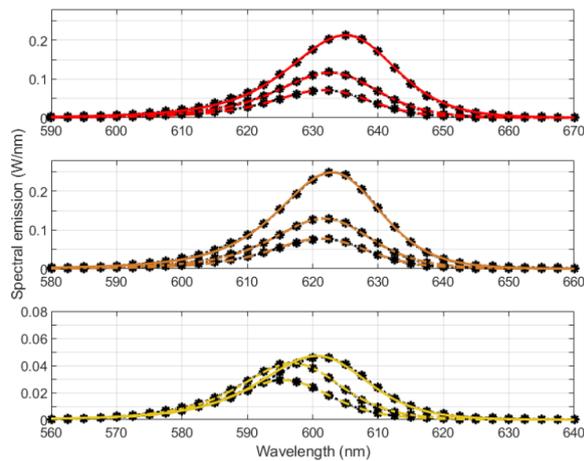
Figure 31: Asymmetric Pearson-VII approximation for Red (upper-panel), Orange (middle-panel) and Amber (lower-panel) LEDs at Idc = 60 mA, 100 mA, and 200 mA. Point values were measured.
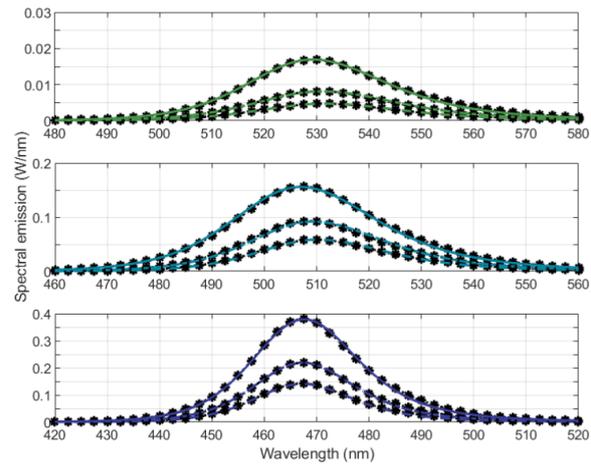
Figure 32: Asymmetric Pearson-VII approximation for Green (upper-panel), Cyan (middle-panel) and Blue (lower-panel) LEDs at Idc = 60 mA, 100 mA, and 200 mA. Point values were measured

2.17 Empirical evaluation of OFDM waveforms for VLC in presence of LED nonlinearities

Researchers: *Mikko Laakso (Aalto University, Finland), Alexis Dowhuszko (Aalto University, Finland), Risto Wichman (Aalto University, Finland).*

Most commercial LEDs found in the market nowadays have been designed for illumination, showing a notable non-linear response when performing the Electrical-to-Optical (E/O) conversion of a multi-carrier waveform for data communication, particularly when using deep Intensity Modulation (IM) indexes for increased useful radiated power. Several different OFDM-based waveforms, adapted to the unipolarity requirement that IM demands, have been proposed in the literature. However, the performance of most of these Optical OFDM waveforms is seriously affected by the non-linear magnitude distortion of white LEDs, particularly when the Peak-to-Average Power Ratio (PAPR) is high. To tackle this issue, this contribution analysed the performance of Constant-Envelope (CE) OFDM, a waveform that modulates the phase of an Intermediate Frequency (IF) carrier with a real-valued OFDM signal before its E/O conversion. The Bit Error Rate of CE-OFDM was compared to the one of DC-biased Optical OFDM (DCO-OFDM) and passband OFDM using a software-defined VLC demonstrator. It was shown that CE-OFDM is more suitable for high energy-efficiency regimes, thanks to its robustness against LED nonlinear responses.

Fig. 33 shows the effect of the LED non-linear distortion according to the received signal constellations (64-QAM in this case), which is highest for DCO-OFDM, moderate for passband-OFDM, and lowest for CE-OFDM. As expected, the effect of the LED non-linearity was minimal for CE-OFDM as the PAPR in this case was the lowest of the three OFDM-based waveforms under analysis.

2.18 An Equivalent Circuit Model of a Commercial LED With an ESD Protection Component for VLC

Researchers: *Xicong Li (Optical Communications Research Group, Faculty of Engineering and Environment, Northumbria University, Newcastle, UK), Zabih Ghassemlooy (Optical Communications Research Group, Faculty of Engineering and Environment, Northumbria University, Newcastle, UK), Stanislav Zvanovec (Department of Electromagnetic Field, Faculty of Electrical Engineering, Czech Technical University, Prague, Czech Republic), and Luis Nero Alves (Instituto de Telecomunicações and*
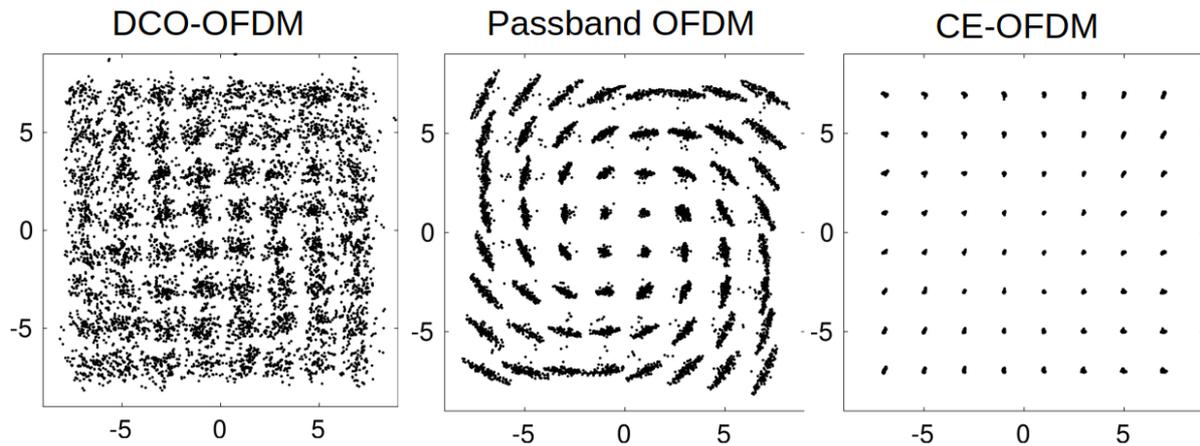
Figure 33: Received constellations for the three OFDM waveforms with same DC-bias, AC-gain, and RMS amplitude of input signal ($\sigma_X = 0.3$).

Departamento de Eletrónica Telecomunicações e Informática, Universidade de Aveiro, Aveiro, Portugal)

An equivalent circuit model for a typical commercial light-emitting diode (LED) used in visible light communication (VLC) applications is proposed. The parameters of the elements in the model are extracted from the measured impedance using a vector network analyser. The model shows high accuracy in fitting the measured results and shows the effect of bonding/packaging parasitics and the electrostatic discharge (ESD) component on the LED's impedance and bandwidth. This study aims to raise the designer's awareness when designing and fabricating high-speed LED/µLED devices to achieve the optimal modulation bandwidth in emerging VLC applications.

The key findings are shown in the following figures. Fig. 34 shows the LED's equivalent circuit model, and Fig. 35 demonstrates the good agreement between the measured and simulated LED impedance. Furthermore, we showed that the predicted frequency response matched the measured S21-parameter, indicating that the bonding parasitics prevent the LED from achieving high bandwidth in the middle-frequency range while the ESD diode introduced steep attenuation slopes in the high-frequency range. The proposed method based on the equivalent circuit model and S-parameters measurement can be applicable to characterising future high-speed LED/µLED devices customised for VLC systems. Finally, experimental investigation demonstrated the effectiveness of the method and provided a set of real-world data for future references.
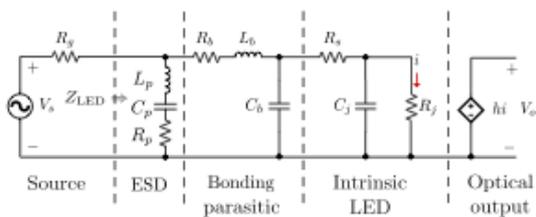
Figure 34: The equivalent circuit model of the LED driven by a source with an output impedance $R_g = 50\,\Omega$.
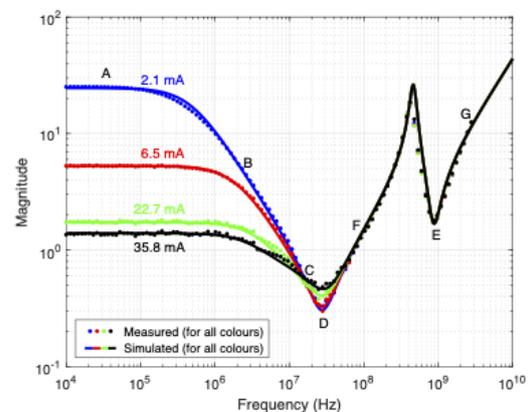
Figure 35: Measured and simulated LED impedance

2.19 Design of MAC-layer Protocols for Distributed NOMA-based VLC Networks

Researchers: *Konstantinos G. Rallis (Aristotle University of Thessaloniki, Greece), Vasilis K. Papaniko-laou (Aristotle University of Thessaloniki, Greece), Panagiotis D. Diamantoulakis (Aristotle University of Thessaloniki, Greece), Alexis A. Dowhuszko (Aalto University, Finland), Jyri Hämäläinen (Aalto University, Finland), George K. Karagiannidis (Aristotle University of Thessaloniki, Greece)*

This contribution investigates a visible light communication (VLC) cellular network that utilizes non-orthogonal multiple access (NOMA) is investigated. To deal with the high inter-cell interference attributed to the high-density of VLC network nodes, a medium access control (MAC) scheduler is designed based on a distributed NOMA approach that aims at increasing the performance of cell-edge users, while securing the high data rate requirements of cell-center users in the VLC network. To this end, two practical protocols are proposed to guarantee the increased spectral efficiency and interference mitigation through distributed NOMA. In each protocol, the decoding strategy and power allocation of the users is investigated through a low complexity algorithm that ensures user fairness in the network.
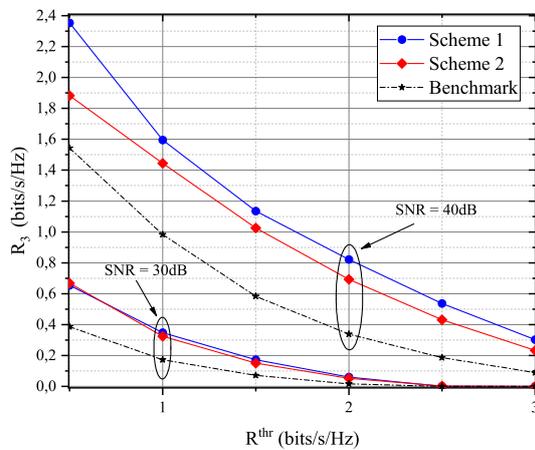
Figure 36: Data rate of the secondary user (R_3) as function of the QoS constraints of the primary users (R^{thr}).
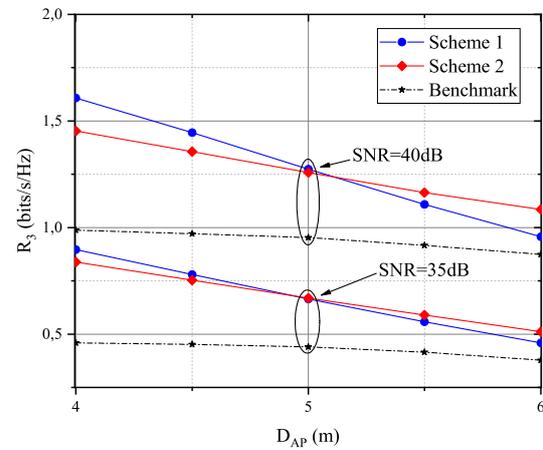
Figure 37: Data rate of the secondary user (R_3) as function of the separation distance between VLC APs (D_{AP}).

In Figure 36, the data rate of the secondary user (R_3) is presented for various cell-center Signal-to-Noise Ratio (SNR) values, $\text{SNR} = (\eta h_0 \mathcal{E})^2 / \sigma^2$, where h_0 is the VLC channel gain when the receiver is directly below the AP (i.e., aligned with the boresight direction of the LED). The impact of the distance between the two APs is evaluated in Figure 37. Interestingly, based on the obtained simulation results reported in this figure, larger distances between the APs made Scheme 2 outperform Scheme 1. This result recommends to design of VLC networks implementing Scheme 2 when APs are located relatively far away. Note that in addition to better performance, Scheme 2 demands less complexity as a lower number of SIC operations are needed.

2.20 Optical Wireless Hybrid VLC/OCC System Based on a Single Centralized LED

Researchers: *Juan Apolo (UPV, Spain), Shivani Rajendra Teli (CTU,Czech), Vicenç Almenar (UPV, Spain), Beatriz Ortega (UPV, Spain), Stanislav Zvánovec (CTU,Czech)*

In recent years OCC have received great attention in the research community and industry due to the large number of smart devices embedding cameras. Furthermore, OCC systems offer stable performance in outdoor environments, the achievable data rate (a few kb/s) is comparatively lower than PD-based systems due to limited camera capture speeds (commonly found as 25 fps).

This contribution proposes the combination of a hybrid VLC/OCC system based on a single centralized

LED to send two data streams of high- and low-speed simultaneously. The detection is based on PDs and image sensors for the high-speed and low-speed stream, respectively. The system aims to provide different services and/or applications to the end-user regardless of the devices employed.

The system combines two signals: (i) a high-speed VLC signal employing a PD as a receiver and; (ii) a low-speed VLC signal employing a camera for detection; which both use a common transmitter designed in a combined manner. Fig. 38 shows a graphical representation of the employed time-dependent signals, where $s(t)$ represents a combination of the high- and low-speed signals and an amplitude overlapping (A_{OL}), i. e. this technique changes the depth of the amplitude of the data signal ON (A_{High}) OFF (A_{Low}). This technique improves the performance of the high-speed signal (improving the bit error rate (BER)) at the cost of degrading the performance of the OCC signal. Two streams of low-speed and high-speed data are simultaneously sent over the optical carrier emitted by a single LED by direct modulation. A step-index POF (SI-POF) network transports the signal, which is then sent over a passive (luminaire-free) FSO link. Thus, the optical front-ends are passive and include only optical lenses for beam collimation to the detector.

In this contribution, we propose and experimentally demonstrate a hybrid VLC/OCC system based on a single centralized LED. In this system, a signal composed of two overlapped data streams of high and low speed is employed to directly modulate an LED emitting at 650 nm. The optical modulated signal is transmitted over a POF with variable length (1-20 m) and a passive optical interface provides the signal adaptation to FSO link (1-3 m). In this system, high speed (up to 88 Mb/s) signal detection is provided by a photodiode and the low-speed stream (up to 4 kb/s) is recovered by an optical camera. System performance satisfies the quality requirements in terms of BER and success of reception (SoR) for VLC and OCC, respectively, and therefore, it is validated for providing multiple services and applications to the end-users in a variety of scenarios while employing a simple and passive optical infrastructure
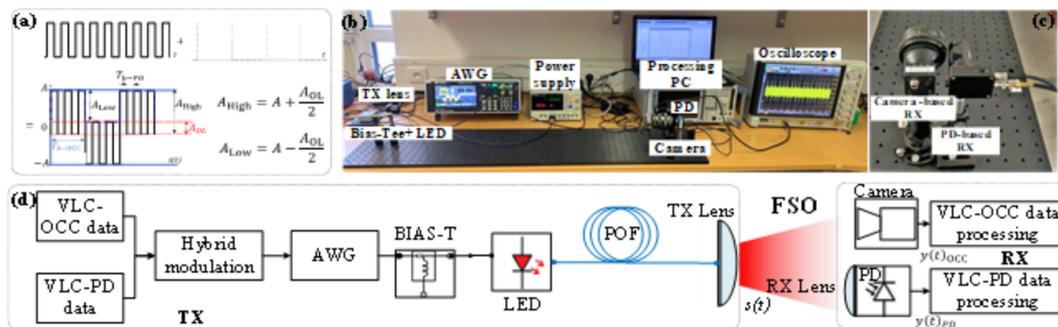
Figure 38: Proposed approach for simultaneous VLC and OCC hybrid transmission: (a) Modulation format, (b) Photograph of the experimental setup, (c) Camera and photodiode installation, (d) Schematic of the laboratory setup.

3 Development of high-accuracy OCC/VLC-based indoor localization

3.1 Experimental Evaluation of a Machine Learning-Based RSS Localization Method Using Gaussian Processes and a Quadrant Photodiode

Researchers: *Elena Aparicio-Esteve (URJC, Spain), Willem Raes (KUL, Belgium), Nobby Stevens (KUL, Belgium), Jesús Ureña (UAH, Spain), Álvaro Hernández (UAH, Spain)*

This work proposes an optical indoor local positioning system based on multiple LEDs and a quadrant photodiode plus an aperture as illustrated in Fig.39. Different frequencies are used to allow the simultaneous emission of all the transmitted signals and their processing at the receiver. For that purpose, two algorithms are developed. First, a triangulation algorithm based on Angle-of-Arrival (AoA) measurements, which uses the Received Signal Strength (RSS) values from every LED on each quadrant to determine the image points projected from each emitter on the receiver and, then, implements a Least Squares Estimator (LSE) and trigonometric considerations to estimate the receiver's position. Secondly, the performance of a data-driven approach using Gaussian Processes (GP) is evaluated. The proposals have been experimentally validated in an area of 3×3 m^2 and a height of 1.3 m (distance from transmitters to receiver). From the conducted experiments and results, it can be concluded that the data-driven method delivers more robust and accurate positioning in the 2D case. When evaluated over the entire area, the AoA method achieves a p50 error of 9.38 cm and a p95 error of 21.94 cm, whereas the GP model obtains a p50 error of 3.62 cm and a p95 error of 16.65 cm, as shown in Fig.40. Another important conclusion is that the GP is capable of delivering robust results in the test area 2 (corner of the setup) with a p50 error of 3.36 cm and a p95 error of 10.35 cm, whereas the p50 and p95 errors for the analytical method are 14.32 cm and 18.56 cm, respectively, in that area. Finally, the analytical method can provide 3D positioning without requiring additional training data, whereas the GP model would require additional observations at different z-coordinates to achieve this.
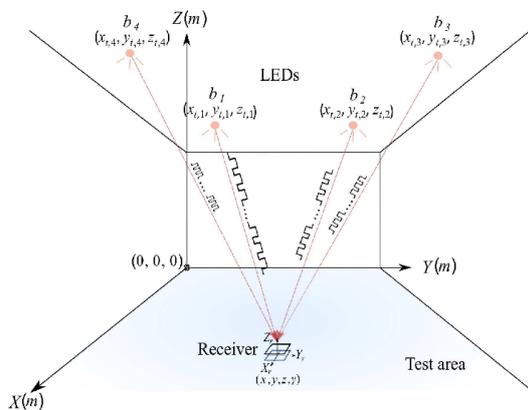
Figure 39: Global overview of the proposed VLP system. Four LEDs placed in the ceiling of the room transmit a modulated signal (each LED at a different frequency) so that the receiver can distinguish their corresponding signal strength.
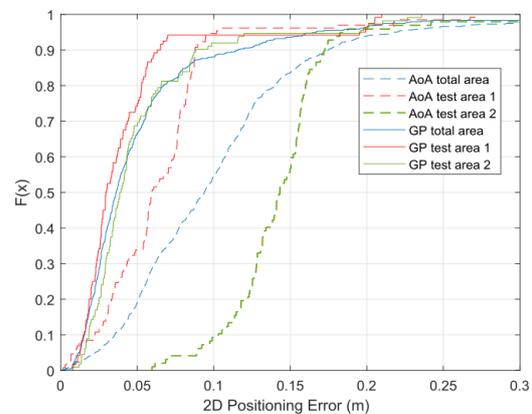
Figure 40: CDF of the global 2D absolute error using AoA and ML techniques.

3.2 Visible Light Positioning and Robotic Platforms: Integration With ROS

Researchers: *Miguel Rêgo (Instituto de Telecomunicações - Aveiro, Portugal), Joaquin Perez (Universitat de València, Spain), Vicent Girbés (Universitat de València, Spain), Luis Alves (Instituto de Telecomunicações - Aveiro, Portugal), Pedro Fonseca (Instituto de Telecomunicações - Aveiro, Portugal)*

The adequate and efficient positioning of autonomous mobile platforms such as AGVs is a challenge for the industry 5.0. In this respect, the feasibility of incorporating communication techniques that improve the current real-time positioning algorithms and enhance the capabilities of this equipment has been

analysed and proposed in a research collaboration between Universitat de Valencia and IT Aveiro. This research focused on the possibilities offered by optical camera communication (OCC) technologies and their applications to visible light positioning (VLP). Moreover, it explored the integration of this type of systems with the Robot Operating System (ROS) platform. The electronic engineering department of University of Valencia and the IT Aveiro are collaborating on the development of a specific framework to integrate OCC based VLP capabilities on robotic platforms.

The work developed focused on exploring techniques for position estimation using visible light sources as the references and a camera as the receiver. More specifically, the goal was to test the existing testbed consisting of LED light sources and current drivers for use in the context of camera based VLP. This was done by assessing the light signal quality using a photodiode and, after that, using a rolling shutter camera. For the latter, an image processing algorithm was developed in order to extract the transmitted information from the striped pattern on the images, thus recovering the identifier of each visible fixture. An example of the isolated fixtures from an image with the modulated patterns is depicted in Fig. 41.

Afterwards, the work focused on integrating the proposed algorithms with the ROS platform. As a tool to facilitate robotics development, ROS provides an open source platform to easily manage and integrate all sensors and actuators in a robotic environment. The proposed algorithms were included on a specific ROS node to be used on a Raspberry Pi controlling a robot, improving the capabilities of the system with VLP accuracy. Finally, the proposed algorithms have been experimentally validated on a dedicated testbed with LED panels from PROEMISA (lighting company) and a robotic arm manipulator, all connected to be managed under the new proposed framework. The manipulator used is shown in Fig. 42, as well as the Raspberry Pi and the Pi Camera attached. That will provide a consistent and comparable system to test future improvements on this area and new collaborations for the NEWFOCUS partners under these new facilities for robotic platforms and OWC.
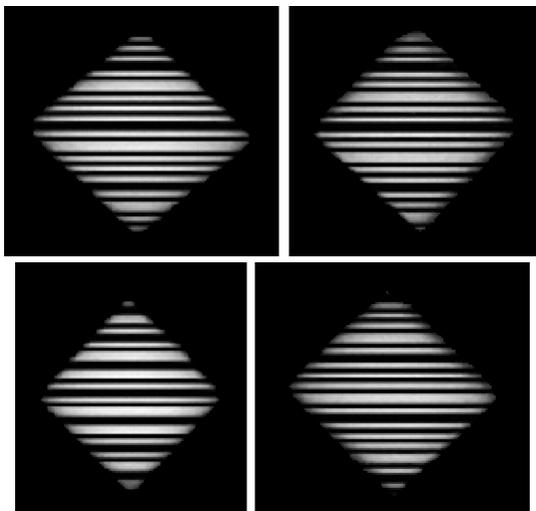
Figure 41: Example of the detected and cropped regions of interest.

Figure 42: Robotic arm used in the experimental process.

3.3   Performance evaluation of VLC-based sensing and localization

Researchers: *Alexis Dowhuszko (Aalto University, Finland), Mehmet Ilter (Aalto University, Finland).*

This contribution studied the effect that the color temperature of an LED lamp has on the ability of a Visible Light Communication (VLC) system to detect different events, which could be the presence, position, and/or color of an object in the sensing area. The proposed VLC-based monitoring system takes

advantage of the Channel State Information (CSI) that the VLC receiver estimates regularly for OFDM equalization, and makes use of an unsupervised learning algorithm to estimate the number of events that can be identified in the collected CSI data. More precisely, the K-means++ clustering algorithm was used to exploit the hidden signatures that discrete events (i.e., color objects) create on the CSI that the VLC system estimates for communications purposes. The color temperature of the LED lighting was varied by changing the fraction of the total radiant flux emitted by Cool-White and Red-Orange LEDs, respectively, enabling to obtain a complete palette of white light that ranges from warm reddish (2600 K) to cool blueish (6200 K). The experimental evaluation was carried out with the aid of a software-defined VLC demonstrator, and showed that the sensing performance when using the reflected VLC signal to estimate the position of the object does not vary notably with the color temperature of the LED lamp. In contrast, the use of white light with high Color Rendering Index provided better results when the objective was to identify the color signature that different objects create. Fig. 43 presents the Overall Accuracy (ACC) of the unsupervised learning classifier in presence of Cool-White illumination (upper panel) and Red-Orange-plus-Cool-White illumination (lower panel), when the Red, Green, and Blue color objects were placed in the eight positions under evaluation in the sensing area. The ACC was evaluated when the same color object was used in the different positions, or when the color of the object was also changed with the given position. According to the bar chart, the accuracy of the classifier degrades slightly as the distance from the LED/PD to the object grows but, in general, was very good for both light sources (i.e., Cool- and Warm-White). Fig. 44 shows the performance of the clustering algorithm when identifying the color signature that an object in a known position introduce on the reflected light. For this purpose, the ACC when the color objects take the eight proposed positions on the sensing area is shown. Note that unlike in the position estimation experiment, the type of illumination source did actually have a notably effect on the identification of the reflected color signature.
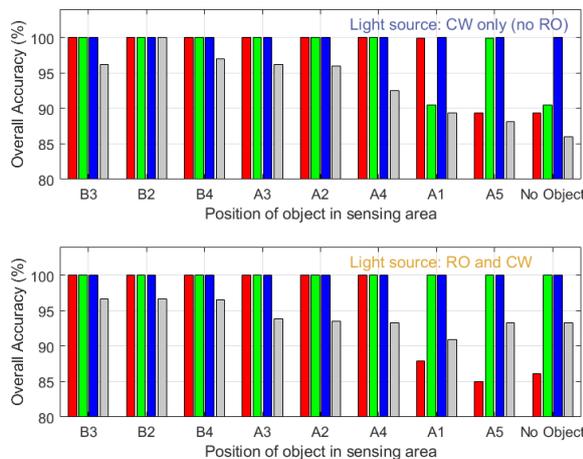
Figure 43: Performance of unsupervised learning for identification of position of objects in the sensing area. Upper panel: Cool-White illumination. Lower panel: Red-Orange- plus-Cool-White illumination. Light Gray bar: Equal-share mixture of Red, Green, and Blue objects.
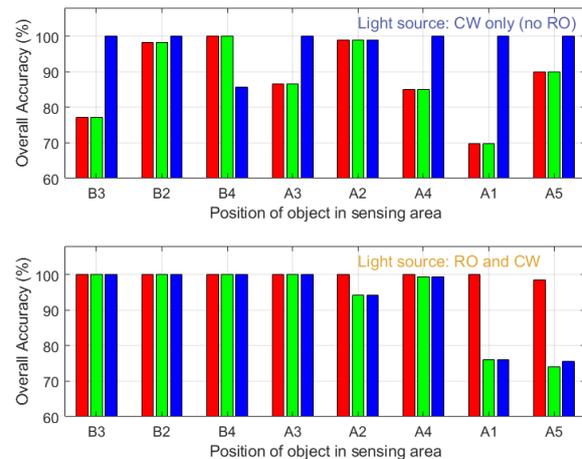
Figure 44: Performance of unsupervised learning for identification of color signature of object in known position. Upper panel: Cool-White illumination. Lower panel: Red-Orange-plus-Cool-White illumination. Red/Green/Blue bars: Given color object in the stated position.

4 Sensing techniques in indoor and outdoor smart environments

4.1 CMOS camera as optical real-time oscilloscope

Researchers: *Lorenzo Gilli (Scuola Superiore Sant'Anna, Italy), Giulio Cossu (Scuola Superiore Sant'Anna, Italy), Ernesto Ciaramella (Scuola Superiore Sant'Anna, Italy)*

Recently, Visible Light Communication (VLC) technology has shown a high potential. However, the absence of a widely accepted standard and the lack of integrated solutions, so far prevented its adoption in the mass market. To overcome this issue, Optical Camera Communication (OCC) was proposed, but still no methodology that gives the deep assessment of a camera as a communication device has been presented. In this work, we introduce a new approach to fully assess the impact of camera detection as an optical receiver for OCC, modelling it as an optical RTO. We present a set of measurements that we apply to a CMOS camera and are based on the standard procedure to characterize an RTO, allowing to quantitatively characterize it. Each pixel of a CMOS camera has a photodiode (PD) that converts the power of the detected light into a voltage by the readout circuitry. Then, an ADC transforms the amplified voltage signal into a set of 16 bits (raw data). To save storage, image compression algorithms (e.g., JPEG) are commonly used. Most commercial CMOS sensors use the Rolling Shutter (RS) readout method, in which the pixels are sampled row-by-row; each row is exposed for a time t_{exp} and collected in a readout time t_{RO}. Therefore, a sinusoidal change in the intensity can result into a regular pattern of fringes in the image, from which the modulation frequency can be effectively obtained. By summing the resulting pattern of fringes along the RS axis, we obtain a profile that shows the light intensity profile across the CMOS sensor (see Fig. 45). In the following measurements, as optical source we used an array of 7 LEDs generating white light. The LEDs were driven in current by a sinewave generated by a waveform generator. The optical signal was sampled and stored by the front camera of a commercial smartphone and analysed by a MATLAB script running on a PC. A diffuser blurred the image and spread quite uniformly the light throughout the sensor. To characterize the CMOS sensor, we perform a set of measurements equivalent to those commonly used for the RTOs. We measure the RTO parameters indispensable to determine the signal integrity: sampling rate, bandwidth, SNR and other parameters and figures of merit. We estimated the sampling rate of the CMOS camera using the relation between sampling rate and readout time. This quantity can be estimated using the profile of the photo when the optical source is modulated by a tone at a defined frequency. To measure the equivalent bandwidth of the CMOS camera, we measured the amplitude of the generated tones at different frequencies, and we acquired the curves as a function of optical attenuation and exposure time (see Fig. 46). The 3-dB bandwidth of the CMOS camera results to be in the range 5-30 kHz and is inversely proportional both to the exposure time and the optical attenuation. A major difference from common RTOs, is that in the optical camera the bandwidth strongly depends on the average intensity of the incident light: the operations for the JPEG compression work as a low-pass filter and are particularly effective for low illumination, in which the higher frequencies are strongly attenuated. SNR depends on noise and distortion, signal power and harmonic distortion. We obtained two curves for two different ISO values. Both curves decrease with the signal frequency. The difference between the curves is only due to the noise amplified by the ISO gain.

4.2 Indoor monitoring system based on ARQ signaling generated by a Visible Light Communication link

Researchers: *Joan Bas (Centre Tecnologic de Telecomunicacions de Catalunya, Spain), Alexis Dowhuszko (Aalto University, Finland).*

One of the main drawback that Visible Light Communications (VLC) systems have when compared to wireless communications on Radio Frequency (RF) bands is that, in presence of obstacles between the transmitter and the receiver, full-blockage events are more likely to happen. This contribution takes advantage of this phenomenon and study the effect that different activities performed by people in the
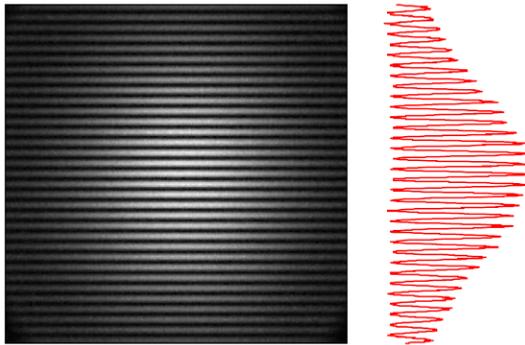
Figure 45: Rolling shutter effect and the corresponding profile in red
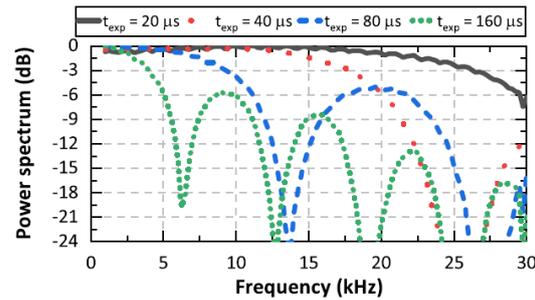
Figure 46: Bandwidth at different exposure time values

service area to-be-monitored have on the Automatic Repeat Request (ARQ) signaling of the VLC link. This study focused on the Stop-and-Wait ARQ protocol, which transmits one data block at a time and waits until a positive (ACK) or negative (NACK) confirmation of the reception of the data packet is signaled to the transmitter. It was noted that in normal working conditions, where no obstacle is placed between the VLC transmitter and receiver, ACKs are mainly received. However, in case of partial VLC link blockage, the SINR of the received signal is reduced, and NACKs start to appear according to the probability of bit error that the VLC link has. Finally, in case of full-blockage, the preamble of the VLC frame cannot be detected and, due to that, no (N)ACKs are issued by the receiver; in this situation, the time-out timer of the transmitter expires continuously until the VLC link can be recovered. Based on experimental studies, it was possible to conclude that different events can be detected correctly according to collected ARQ signaling statistics.

Fig. 47 shows the corresponding time-to-ACK (i.e., the time that takes to receive the ACK message of a data block) for different activities. If a person walks, then the duration of the time-to-ACK augmented with respect to the running case. When a person with crutches (or when two people) walking obstruct the VLC link, the time-to-ACK increased even more than before. Fig. 48 shows the Cumulative Distribution Function (CDF) of the number of time-outs and NACKs when a walking person obstructed the LED-to-wall and wall-to-PD beams. The number of time-outs when blocking took place in the LED-to-wall beam was lower than the ones that would correspond when blocking the wall-to-PD beam. In contrast, when measuring the number of NACKs, the opposite effect takes place. The reason for this behavior is that expected event in the first beam was *full-blockage* (smaller beam size) whereas, in the second beam, the dominant event was most likely a *partial-blockage* (larger beam size).

4.3 Visible Light Communications: A novel indoor network planning approach

Researchers: *Mohsen Abedi (Aalto University, Finland), Alexis Dowhuszko (Aalto University, Finland), Risto Wichman (Aalto University, Finland)*.

Visible Light Communications (VLC) systems offer a low-cost technology on license-free spectrum to complement the contemporary mobile network services offered on Radio Frequency (RF) bands. However, VLC signals suffer from propagation limits when compared to RF ones. Firstly, in presence of opaque obstacles such as walls, doors, and even curtains, strong link blockage is experienced as the power of reflections is much weaker than the power of the Line-of-Sight (LoS) link. Secondly, the received optical power in the mobile user drops as the angle of irradiance between a LED lamp and the user increases, imposing a range constraint on the VLC nodes that depends on the Field-of-View (FoV) angle of the Photodetector (PD). This contribution proposed a Partition-based Visibility (PV) graph modelling to find the minimum number of VLC nodes and their locations for reliable indoor coverage. Inspired by the Art Gallery Problem, the number and the locations of VLC nodes was optimized by characterizing the
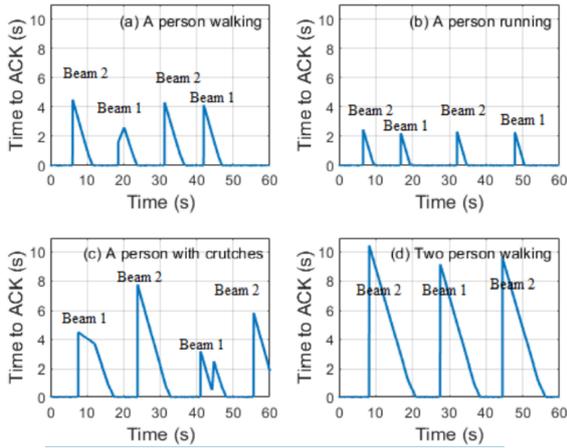
Figure 47: Time-to-ACK observed in the VLC link when: a) A person walking; b) A person running; c) A person walking with crutches; d) Two people walking.
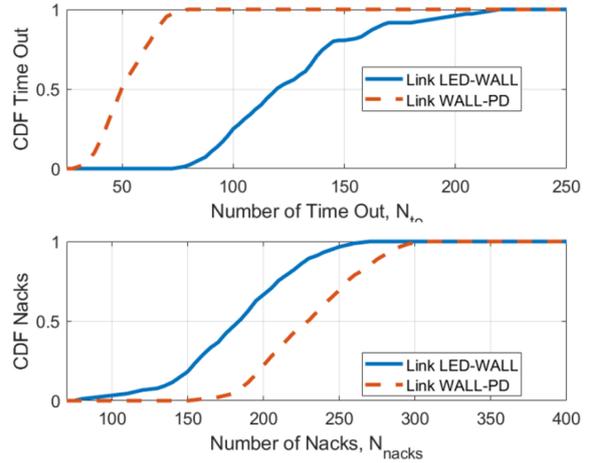
Figure 48: Cumulative Distribution Function (CDF) for time-outs (upper panel) and NACKs (lower panel) originated in LED-to-wall and wall-to-PD beams.

PV graph as a dual presentation of the floor plan and a Maximal Clique Clustering algorithm, which was able to solve not only the art gallery problem but also to extend the approach for the range-constrained case.

Fig. 49 shows the minimum number of VLC nodes that are needed to cover the layout as a function of the maximum range of a VLC cell. It is observed that similar to unconstrained case, setting the range $r \geq 6.2\,\mathrm{m}$ results in only three nodes, whereas setting $r = 4.8$, 3.6 and $2.8\,\mathrm{m}$ results in four, five, and seven VLC nodes, respectively. On the other hand, assuming that the VLC users are randomly distributed in the layout, Fig. 50 shows the Cumulative Distribution Function (CDF) of user distances for the four representative cases. The deployment of four nodes (green curves) outperformed the three nodes deployment (red curves) by reducing the 90-th percentile as much as $2\,\mathrm{m}$. Moreover, when deploying five nodes (blue curves) and seven nodes (magenta curves), there was still a decrease in the 90-th percentile which was more modest than before.
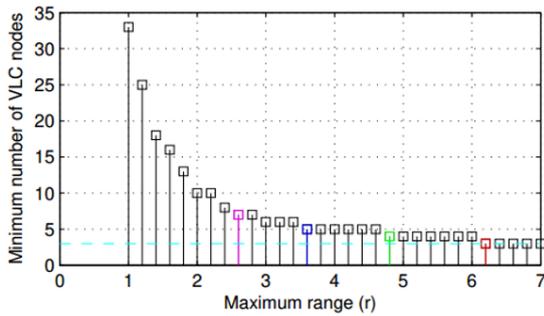
Figure 49: Effect of the maximum range of a VLC node on the network planning procedure. Minimum number of VLC nodes required to cover the service layout is shown as function of VLC ranges.
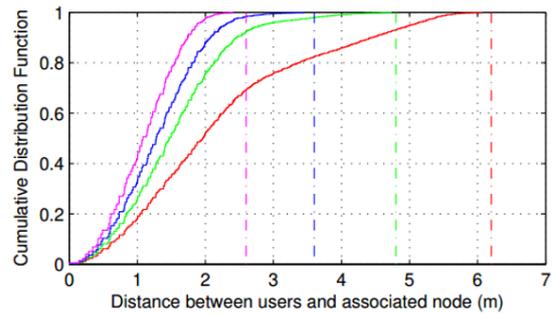
Figure 50: CDF of user distances to the nearest VLC nodes in the given service layout for four representative maximum VLC cell ranges (red: $6.2\,\mathrm{m}$; green: $4.8\,\mathrm{m}$; blue: $3.6\,\mathrm{m}$; magenta: $2.6\,\mathrm{m}$).

References

[1] Sylvester Aboagye, Telex M. N. Ngatched, Octavia A. Dobre, and Alain R. Ndjiongue. Intelligent Reflecting Surface-Aided Indoor Visible Light Communication Systems. *IEEE Communications Letters*, 25(12):3913–3917, dec 2021.

[2] Lei Qian, Xuefen Chi, Linlin Zhao, and Anas Chaaban. Secure Visible Light Communications via Intelligent Reflecting Surfaces. In *ICC 2021 - IEEE International Conference on Communications*, pages 1–6. IEEE, jun 2021.

[3] Wasiu O. Popoola, Evangelos Pikasis, and Isaac Osahon. Hybrid polymer optical fibre and visible light communication link for in-home network. *2017 26th Wireless and Optical Communication Conference, WOCC 2017*, (Mc):2–7, 2017.

[4] Sepideh Mohammadi Kouhini, Sreelal Maravanchery Mana, Peter Hellwig, Jonas Hilt, Dominic Schulz, Anagnostis Paraskevopoulos, Ronald Freund, and Volker Jungnickel. Performance of Bidirectional LiFi over Plastic Optical Fiber (POF). In *2020 12th International Symposium on Communication Systems, Networks and Digital Signal Processing, CSNDSP 2020*. Institute of Electrical and Electronics Engineers Inc., jul 2020.

[5] Carina Ribeiro Barbio Corrêa, Ketema Addis Mekonnen, Frans Huijskens, Ton Koonen, and Eduward Tangdiongga. Passive OFE multi-Gbps VLC transmission using POF as a feeder line. *Microwave and Optical Technology Letters*, may 2022.

[6] Juan Andrés Apolo, Beatriz Ortega, and Vicenç Almenar. Hybrid POF/VLC Links Based on a Single LED for Indoor Communications. *Photonics*, 8(7):254, jul 2021.

[7] Isaac N. Osahon, Evangelos Pikasis, Sujan Rajbhandari, and Wasiu O. Popoola. Hybrid POF/VLC link with M-PAM and MLP equaliser. In *2017 IEEE International Conference on Communications (ICC)*, pages 1–6. IEEE, may 2017.

[8] Chun-Yu Lin, Chung-Yi Li, Hai-Han Lu, Ching-Hung Chang, Peng-Chun Peng, Chia-Rung Lin, and Jian-Hua Chen. A Hybrid CATV/16-QAM-OFDM In-House Network Over SMF and GI-POF/VLC Transport. *IEEE Photonics Technology Letters*, 27(5):526–529, mar 2015.

[9] M. Wolf and M. Haardt. On the DC balance of multi-level PAM VLC systems. In *21th International Conference on Transperent Optical Networks (ICTON) 2019*, Angers, France, June 2019.

[10] S. Mardani and J.P. Linnartz. Capacity of the first-order low-pass channel with power constraint. In *Proceedings of the 2018 Symposium on Information Theory and Signal Processing in th Benelux*, pages 149–153, 2018.